THE JOURNAL OF PHYSICAL CHEMISTRY B
A JOURNAL OF THE AMERICAN CHEMICAL SOCIETY

pubs.acs.org/JPCB

Article

Compositional Evolution of the Structure and Connectivity in Binary P−Se Glasses: Results from 2D Multinuclear NMR and Raman Spectroscopy

Bing Yuan, Bruce Aitken, Ivan Hung, Zhehong Gan, and Sabyasachi Sen*

Cite This: *J. Phys. Chem. B* 2021, 125, 13057−13067

Read Online

ACCESS | Metrics & More | Article Recommendations

ABSTRACT: The atomic structure of binary P_xSe_{100-x} glasses with $5 \leq x \leq 70$ is investigated using Raman spectroscopy and two-dimensional ^{77}Se and ^{31}P isotropic/anisotropic correlation nuclear magnetic resonance (NMR) spectroscopy. These spectroscopic results, when taken together, demonstrate that the structure of P_xSe_{100-x} glasses with $x \leq 50$ consists primarily of −Se−Se−Se− chain elements, pyramidal $P(Se_{1/2})_3$ units, ethylene-like $_{2/2}SeP-PSe_{2/2}$ units, and $Se{=}P(Se_{1/2})_3$ tetrahedral units. The chain structure of Se becomes increasingly cross-linked by P−Se polyhedral units, and the degree of connectivity increases with a progressive increase in P content up to $x \sim 50$, at which point the −Se−Se−Se− chain elements completely disappear, and the structure becomes highly rigid. The compositional variation of the Se−**Se**−Se environments as obtained from the ^{77}Se isotropic NMR spectra reveals that the connectivity between the Se−Se and P−Se units in glasses with $x \leq 50$ is intermediate to that of the random and the fully clustered scenarios. A further increase in P content results in the formation of P_4Se_3 molecules such that at $x = 63$, the structure becomes predominantly molecular, consisting of P_4Se_3 molecules likely held together via van der Waals forces. The structure of glasses with $x > 63$ is characterized by P_4Se_3 molecules and likely nonmolecular P_4Se_3-like species, along with amorphous red phosphorus-like regions. These P_4Se_3-like moieties and the amorphous red phosphorus-like units can connect to each other via P−P bonds, and their relative concentrations increase with increasing P content. This compositional evolution of structural connectivity of P_xSe_{100-x} glasses is shown to be consistent with the corresponding variation in the glass transition temperature.

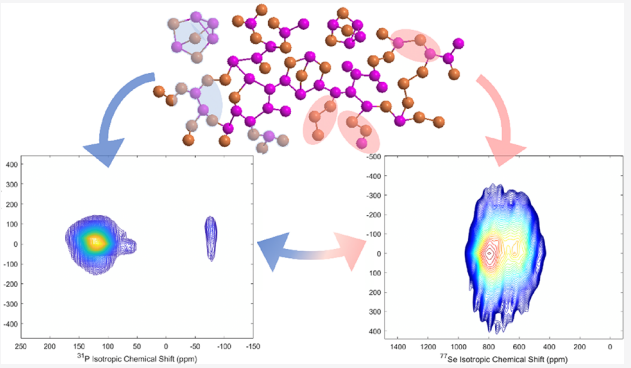

1. INTRODUCTION

Chalcogenide crystals and glasses have found important technological applications in the areas of infrared photonics, phase change memory, and remote sensing.[1−5] More recently, crystals in the P−Se system have been found to be highly efficient as an anode material for solid-state Na-ion batteries.[6,7] The unusually large composition range for bulk glass formation and the complex compositional variation of the structural building blocks make the binary P−Se system somewhat unique among glass-forming chalcogenides. Consequently, the structure of P−Se glasses has been investigated extensively in the past decades using a wide range of techniques including Raman scattering, neutron diffraction, X-ray absorption, and nuclear magnetic resonance (NMR) spectroscopy.[8−15] Bulk glass formation in the P−Se binary system is reported in the composition range 0 at % ≤ P ≤ 80 at % with a narrow gap centered around 57 at % P corresponding to the stoichiometry of P_4Se_3 molecules.[16] Previous Raman scattering and ^{31}P magic-angle-spinning (MAS) and two-dimensional (2D) J-resolved NMR spectroscopic studies[8−10,15] have provided a detailed picture of the identification and the composition-dependent evolution of relative fractions of the constituent P-centric coordination polyhedra and short-range structure of P−Se glasses. The structure of the Se-rich glasses (≤20 at % P) consists of Se chains interconnected primarily by $Se{=}P(Se_{1/2})_3$ tetrahedra and $P(Se_{1/2})_3$ pyramids. As the P content increases beyond 30 at %, the P atoms exist predominantly in the form of $P(Se_{1/2})_3$ pyramids and $_{2/2}SeP-PSe_{2/2}$ ethylene-like units, whereas in P-rich glasses with >50 at % P, the P atoms are incorporated in P_4Se_3 (and possibly P_4Se_2) molecules and also form amorphous red phosphorus-like structural moieties.[9] Therefore, the structure of P−Se glasses evolves, with increasing P content, from linear chains to highly cross-linked

Received: August 27, 2021
Revised: November 3, 2021
Published: November 18, 2021

networks all the way to zero-dimensional molecules and finally to molecules embedded in a polymeric matrix. Such structural complexity including the violation of the $8 - N$ rule for P coordination, strong violation of chemical order via the formation of P−P homopolar bonds even in Se-excess glasses, and the formation of predominantly molecular glasses can be contrasted with the relative structural simplicity of selenide glasses containing conventional cross-linkers such as As or Ge that do not display such behavior. Although the evolution of the short-range structure of binary P−Se glasses in terms of the P speciation has been studied extensively throughout the glass formation range, little is known regarding the speciation of the Se environments and the intermediate-range order in terms of the connectivity between the constituent structural units. In this regard, the only systematic study, to the best of our knowledge, was carried out by Eckert et al.[17] In this study, the intermediate-range order of P−Se glasses was described in terms of the connectivity between the Se−Se segments and the P-containing building blocks on the basis of the results from ^{31}P−^{77}Se spin echo double resonance (SEDOR) and *in situ* high-temperature ^{77}Se wideline NMR spectroscopy.[17] Their results were shown to be consistent with a model of random connectivity between these structural moieties. However, such a conclusion could not be experimentally verified without the direct knowledge of Se speciation in these binary P−Se glasses due to the lack of high-resolution ^{77}Se NMR data. High-resolution ^{77}Se NMR spectroscopy in chalcogenide glasses remains challenging owing to the low natural abundance of ^{77}Se (∼7%), its long spin−lattice relaxation time, large chemical shift range, and chemical shift anisotropy (CSA). The last two problems can be addressed effectively via the application of the 2D magic-angle-turning phase-adjusted spinning sidebands (MATPASS) NMR technique, which can separate the CSA from the isotropic chemical shift in a separate dimension, thereby avoiding any CSA-related broadening and consequently increasing the spectral resolution in the isotropic dimension.[18] Moreover, the separation of the isotropic shift from CSA allows the use of high magnetic fields for increased sensitivity and resolution without requiring fast spinning of samples in small-volume rotors for CSA averaging.

It may be noted here that the chemical shift δ of a nuclide is a second rank tensor that can be described using the principal components δ_{xx}, δ_{yy}, and δ_{zz}. The isotropic chemical shift δ_{iso} is the average of these three components

$$\delta_{iso} = \frac{1}{3}(\delta_{xx} + \delta_{yy} + \delta_{zz})$$

Following the Haeberlen convention, these principal components are arranged such that[19]

$$|\delta_{zz} - \delta_{iso}| \geq |\delta_{xx} - \delta_{iso}| \geq |\delta_{yy} - \delta_{iso}|$$

More commonly, however, the tensor is reported in terms of δ_{iso}, and the CSA is expressed by the reduced anisotropy Δ and the asymmetry parameter η, which are related to the principal components as

$$\Delta = \delta_{zz} - \delta_{iso}$$

$$\eta = \frac{\delta_{xx} - \delta_{yy}}{\delta_{zz} - \delta_{iso}}$$

The CSA parameters Δ and η represent the deviation of the tensor from spherical and axial symmetry, respectively. While δ_{iso} of a nuclide is characterized of its coordination environment, the CSA carries important complementary information related to the symmetry of its local electronic environment. Therefore, the separation of isotropic and anisotropic chemical shifts in two dimensions makes MATPASS a powerful NMR technique in the investigation of short- and intermediate-range structural order in glasses. Here, we present the results of a comprehensive structural investigation of binary P_xSe_{100-x} glasses with $5 \leq x \leq 70$ using high-resolution 2D ^{77}Se and ^{31}P MATPASS NMR spectroscopy. The composition-dependent evolution of the relative fractions of different Se and P environments as obtained from the analyses of the ^{77}Se and ^{31}P NMR data are used in combination with Raman spectroscopic results to build a more complete model of intermediate-range order and structural connectivity in these glasses.

2. EXPERIMENTAL METHODS

2.1. Sample Preparation and Physical Characterization. Binary P_xSe_{100-x} glasses with x = 5, 10, 20, 25, 30, 35, 40, 45, 50, 63, 67, 70 were prepared in ∼12 g batches from constituent elements using the conventional melt-quench method. Mixtures of red phosphorus (Spectrum, 99.999%) and selenium (Alfa Aesar, 99.999%) were taken in 6 mm inner diameter quartz ampoules that were evacuated (10^{-4} Torr) and flame-sealed prior to loading into a rocking furnace. The ampoules were slowly heated to 923 K over 13 h and held at this temperature for 36 h to ensure melt homogeneity. The ampoules were then quenched in water to obtain the glass samples.

The glass transition temperature T_g of the P_xSe_{100-x} glasses was measured using a differential scanning calorimeter (Mettler-Toledo DSC1). Approximately 15 mg of powdered glass sample was hermetically sealed in a 40 μL aluminum crucible. Scans were performed at 10 °C/min under a continuously flowing nitrogen environment. T_g was determined within ±1 °C as the onset of the glass transition.

2.2. Raman Spectroscopy. The Raman spectra of all glasses were collected in backscattered geometry using a Renishaw 1000 Raman microscope spectrometer equipped with a He-Ne laser operating at a wavelength of 633 nm. Each Raman spectrum was collected at 50% laser power with 1 cm^{-1} resolution. The backscattered light was detected using a charge-coupled device cooled at 200 K.

2.3. NMR Spectroscopy. The 2D ^{77}Se MATPASS/Carr-Purcell Meiboom-Gill (CPMG)[18] and ^{31}P MATPASS[20] NMR spectra for all glasses were acquired at the National High Magnetic Field Laboratory (NHMFL) using a 31 mm bore 19.6 T magnet equipped with a Bruker Avance NEO console operating at resonance frequencies of 158.7 and 336.6 MHz for ^{77}Se and ^{31}P, respectively, and a low-E double-resonance probe. Crushed glass samples were packed into 3.2 mm ZrO_2 rotors and spun at 10 kHz. The ^{77}Se spectra were acquired with $\pi/2$- and π-pulses of 3.0 and 6.0 μs, respectively, and CPMG echo-train acquisition with 159 echoes was acquired for each transient to enhance sensitivity. The method of States et al.[21] for hypercomplex data acquisition was applied to the CPMG pulse phase and the receiver phase simultaneously. The 2D acquisition consisted of 16 hypercomplex t_1 increments each with 24 transients and 110 s recycle delay, for a total experimental duration of 23.5 h per spectrum. The ^{31}P spectra were acquired with $\pi/2$- and π-pulses of 2.6 and 5.2 μs, respectively. The 2D acquisition consisted of 16 complex t_1

https://doi.org/10.1021/acs.jpcb.1c07601
J. Phys. Chem. B 2021, 125, 13057−13067

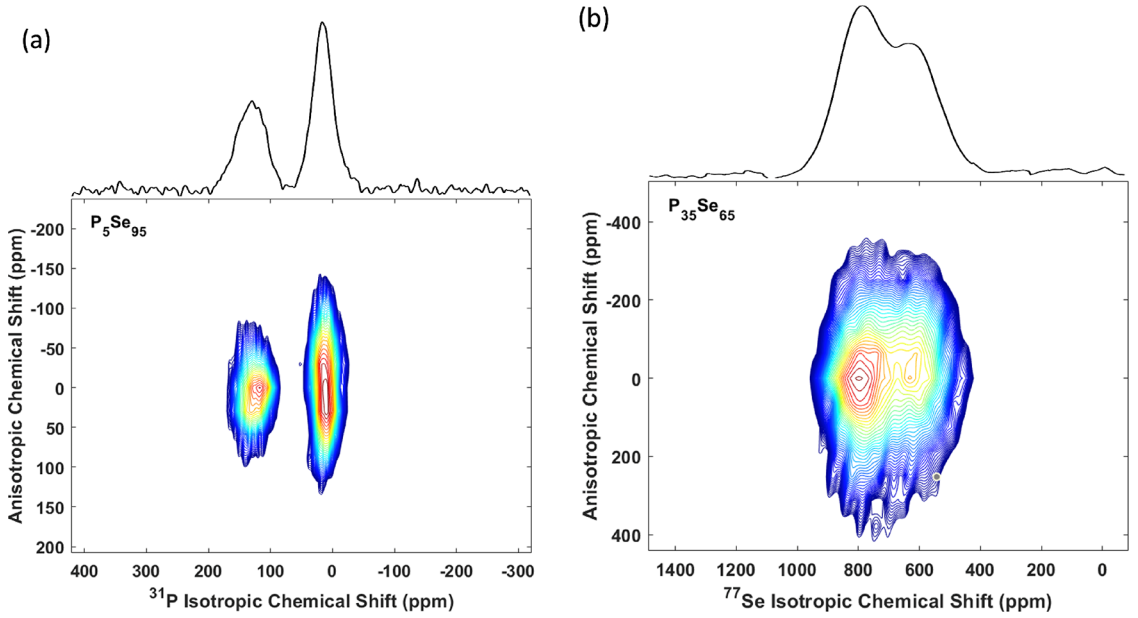

Figure 1. Contour plots of representative (a) ^{31}P MATPASS and (b) ^{77}Se MATPASS/CPMG spectra of P_xSe_{100-x} glasses. Glass compositions are indicated in the insets. Total projections along isotropic dimension are shown on top of each plot (solid black line).

increments each with 12 transients and 240 s recycle delay, for a total experimental duration of 12.8 h per spectrum. The 2D spectra were sheared to an isotropic/anisotropic representation in the direct/indirect dimensions during processing, as detailed in the works of Hung et al.[18,20] Representative 2D ^{31}P and ^{77}Se MATPASS spectra of P_xSe_{100-x} glasses obtained in this study are shown in Figure 1.

^{77}Se MAS and ^{31}P PASS NMR data were collected for the molecule-rich P_xSe_{100-x} glasses with x = 63, 67, and 70. The ^{77}Se MAS spectra were collected at 19.6 T using the NHMFL system described above with a $\pi/2$-pulse of 3.0 μs, 5.0 s recycle delay, and 16 transients averaged per sample. Crushed glass samples were packed into 3.2 mm ZrO_2 rotors and spun at 10 kHz. The ^{31}P PASS spectra were collected at Davis using a Bruker Avance spectrometer operating at 11.7 T (Larmor frequency of 202.4 MHz for ^{31}P) and a Bruker triple resonance MAS probe. Crushed samples were spun at a rate of 6 kHz in 4 mm ZrO_2 rotors. The PASS pulse sequence consisted of a $\pi/2$ pulse (1.95 μs) followed by a train of π pulses. The inter-pulse delays were rotor synchronized according to the solutions of the PASS equations given by Antzutkin et al.[22] All pulses were cogwheel phase cycled to eliminate the effects of pulse imperfections. The 2D acquisition consisted of 32 hypercomplex t_1 increments, each with 12 transients, and a recycle delay of 20 s was used. All ^{77}Se and ^{31}P NMR spectra were externally referenced by recording the ^{17}O signal of natural abundance H_2O and using the appropriate frequency ratios as reported in the IUPAC recommendations.[23] The isotropic and anisotropic spectral line shapes, as obtained from the MATPASS and PASS data, were simulated using the software program DMFit to obtain the relative fractions of the various Se and P environments and their corresponding CSA parameters.[24]

3. RESULTS AND DISCUSSION

3.1. Raman Spectroscopy. The Raman spectra of all P_xSe_{100-x} glasses are shown in Figure 2. The major bands in $x \leq 50$ glass compositions can be readily assigned on the basis of

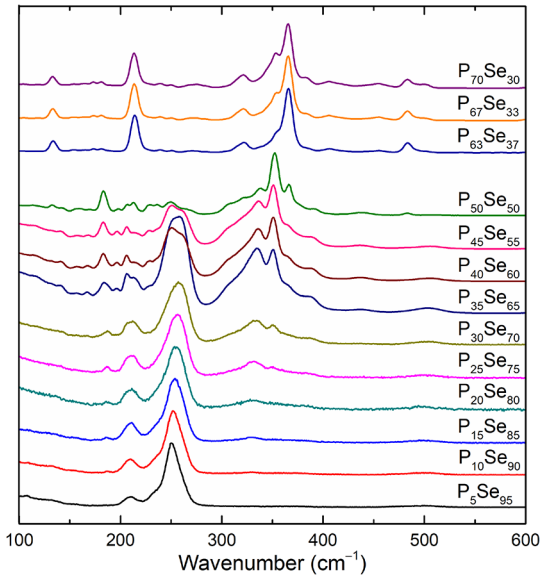

Figure 2. Unpolarized Raman spectra of P_xSe_{100-x} glasses. Glass compositions are listed alongside the spectra.

previous studies[8,10] to the Se−Se stretching mode (~250 cm^{-1}), the symmetric and asymmetric stretching of P−Se bonds in pyramidal $P(Se_{1/2})_3$ units (~330 and 210 cm^{-1}, respectively), the vibrational modes of ethylene-like $_{2/2}$SeP−$PSe_{2/2}$ units (~185, 330−350, and 370 cm^{-1}), and the stretching of the P═Se bonds in Se═$P(Se_{1/2})_3$ tetrahedral units (~500 cm^{-1}). The Se−Se stretching band at ~250 cm^{-1} is the most intense in Se-rich glasses and its intensity decreases continuously with increasing P content, whereas the intensities of the bands corresponding to the P-containing structural moieties concomitantly increase up to 35% P (Figure 2). Above 35 at % P, the intensity of the 185 cm^{-1} band continues to increase, while that of the 210 cm^{-1} band decreases, suggesting the incorporation of an increasing number of P atoms into the ethylene-like $_{2/2}$SeP−$PSe_{2/2}$ units. When taken

https://doi.org/10.1021/acs.jpcb.1c07601
J. Phys. Chem. B 2021, 125, 13057−13067

together, these observations indicate that the Se chains are cross-linked by the various P-containing structural moieties and the average chain length is progressively shortened due to an increasing degree of connectivity of the glass structure. This compositional evolution of the structure of P−Se glasses is in broad agreement with that reported in a previous study by Georgiev et al.[8] However, it may be noted here that, in the Raman spectra reported by Georgiev et al., the 185 cm^{-1} band corresponding to the $_{2/2}SeP-PSe_{2/2}$ unit becomes barely noticeable for the first time in the $P_{20}Se_{80}$ glass, while in the present study, a weak signature of this band can already be seen in the spectrum of the $P_{10}Se_{90}$ glass (Figure 2). This observation in the present study is consistent with the 2D J-resolved ^{31}P NMR spectroscopic results on P−Se glasses reported by Bytchkov et al.,[9] which have conclusively shown that the $_{2/2}SeP-PSe_{2/2}$ units definitely appear in P−Se glasses with >10% P.

Besides the abovementioned bands, new bands located at ∼133, 213, 366, and 484 cm^{-1}, which correspond to the intramolecular modes of P_4Se_3 molecules,[15] appear in the Raman spectrum of the $P_{50}Se_{50}$ glass (Figure 2). These molecular bands dominate the Raman spectra of P−Se glasses with $x \geq 63$, indicating that the P_4Se_3 molecules are a major constituent of the structure of these P-rich glasses (Figure 2). Finally, the appearance of bands at ∼353 and 500 cm^{-1} in the Raman spectra of these P-rich glasses is likely indicative of the formation of amorphous red phosphorus-like structural moieties.[15] Therefore, when taken together, these results suggest that the nanostructure of the P-rich glasses consists of P_4Se_3 molecules coexisting with amorphous red phosphorus-like regions.

3.2. ^{31}P NMR. The ^{31}P isotropic NMR spectra of the P_xSe_{100-x} glasses with $x \leq 50$ display two distinct resonances centered at δ_{iso} ∼129 and 10 ppm with the relative intensity of the former increasing monotonically with increasing P content (Figure 3). Previous ^{31}P NMR studies have shown that the resonance near δ_{iso} ∼10 ppm can be assigned to the tetrahedral $Se{=}P(Se_{1/2})_3$ site while the resonance located at δ_{iso} ∼129 ppm corresponds to P atoms in pyramidal $P(Se_{1/2})_3$ units.[9,11] These studies were able to show, on the basis of ^{31}P dipolar NMR and 2D J-resolved ^{31}P NMR spectroscopic results, that this resonance also contained a signal from P in $_{2/2}SeP-PSe_{2/2}$ units with δ_{iso} ∼125 ppm and that, with increasing P concentration, the relative contribution of $_{2/2}SeP-PSe_{2/2}$ units increased compared to that from $P(Se_{1/2})_3$ units. The separation of the ^{31}P isotropic and anisotropic shifts into two dimensions in the MATPASS and PASS NMR spectra obtained in the present study allows for the determination of the chemical shift tensor parameters Δ and η for the P sites from the simulations of the corresponding spinning sideband intensity pattern in the anisotropic dimension (Figure 4). These simulations performed at several δ_{iso} values yield average values of $\Delta = -127 \pm 10$ ppm and $\eta = 0.9 \pm 0.1$ for the tetrahedral $Se{=}P(Se_{1/2})_3$ environment and $\Delta = -78 \pm 10$ ppm and $\eta = 0.8 \pm 0.1$ for the pyramidal $P(Se_{1/2})_3$ and ethylene-like $_{2/2}SeP-PSe_{2/2}$ environments. These ^{31}P chemical shift tensor parameters for all P_xSe_{100-x} glasses are listed in Table 1 and shown in Figure 5. As shown in previous studies, the resonance at δ_{iso} ∼129 ppm is expected to be dominated by the $P(Se_{1/2})_3$ units near $x = 15$, while the $_{2/2}SeP-PSe_{2/2}$ units are expected to dominate near $x = 50$.[9,11] Therefore, if the ^{31}P chemical shift tensor parameters for these two units are significantly different, then one would expect a monotonic

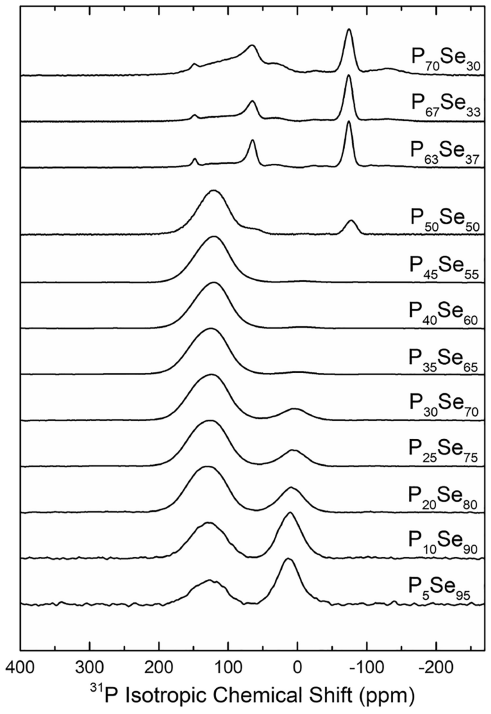

Figure 3. ^{31}P isotropic NMR spectra of P_xSe_{100-x} glasses. Glass compositions are listed alongside the spectra.

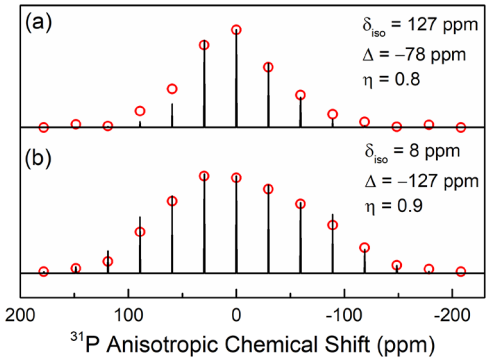

Figure 4. Experimental (empty red circles) and simulated (black traces) ^{31}P NMR spinning sideband intensities in the anisotropic dimension for (a) three-coordinated P sites and (b) four-coordinated P sites in P_5Se_{95} glass at δ_{iso} ∼127 and 8 ppm, respectively.

evolution of the average values of Δ and η in the composition range $15 \leq x \leq 50$. However, it is apparent from Table 1 and Figure 5 that within experimental error, neither Δ nor η shows any significant change with glass composition, although the average absolute value of Δ does appear to increase monotonically from ∼80 to ∼90 ppm with increasing P content in this composition range. Unfortunately, the magnitude of the change in Δ is well within the experimental error (Figure 5), and thus, the observed trend cannot be assigned unequivocally to a replacement of the $P(Se_{1/2})_3$ units with the $_{2/2}SeP-PSe_{2/2}$ units in the structure of these glasses with increasing P content.

Although a full quantitative analysis of composition-dependent variation of the relative fractions of all three types of P environments is prohibited by the complete overlap of the signals from the $P(Se_{1/2})_3$ and $_{2/2}SeP-PSe_{2/2}$ sites in the isotropic ^{31}P NMR spectra, the ratios for three- and four-coordinated P environments in all glass compositions with $x \leq$

https://doi.org/10.1021/acs.jpcb.1c07601
J. Phys. Chem. B 2021, 125, 13057−13067

Table 1. ^{31}P Chemical Shift Anisotropy Parameters for P_xSe_{100-x} Glasses

	3-coordinated P site		4-coordinated P site		apical P site in P_4Se_3		basal P site in P_4Se_3	
	Δ (±10 ppm)	η (±0.1)	Δ (±10 ppm)	η (±0.1)	Δ (±10 ppm)	η (±0.1)	Δ (±10 ppm)	η (±0.1)
P_5Se_{95}	−78	0.8	−127	0.9				
$P_{10}Se_{90}$	−80	0.7	−133	0.9				
$P_{20}Se_{80}$	−80	0.7	−132	0.9				
$P_{25}Se_{75}$	−80	0.7	−133	0.9				
$P_{30}Se_{70}$	−81	0.7	−132	0.9				
$P_{35}Se_{65}$	−83	0.8	−130	0.9				
$P_{40}Se_{60}$	−86	0.7						
$P_{45}Se_{55}$	−88	0.7						
$P_{50}Se_{50}$	−88	0.8					−143	0.8
$P_{63}Se_{37}$					−76	0.6	−140	0.8
$P_{67}Se_{33}$					−77	0.6	−141	0.8
$P_{70}Se_{30}$					−76	0.6	−142	0.8

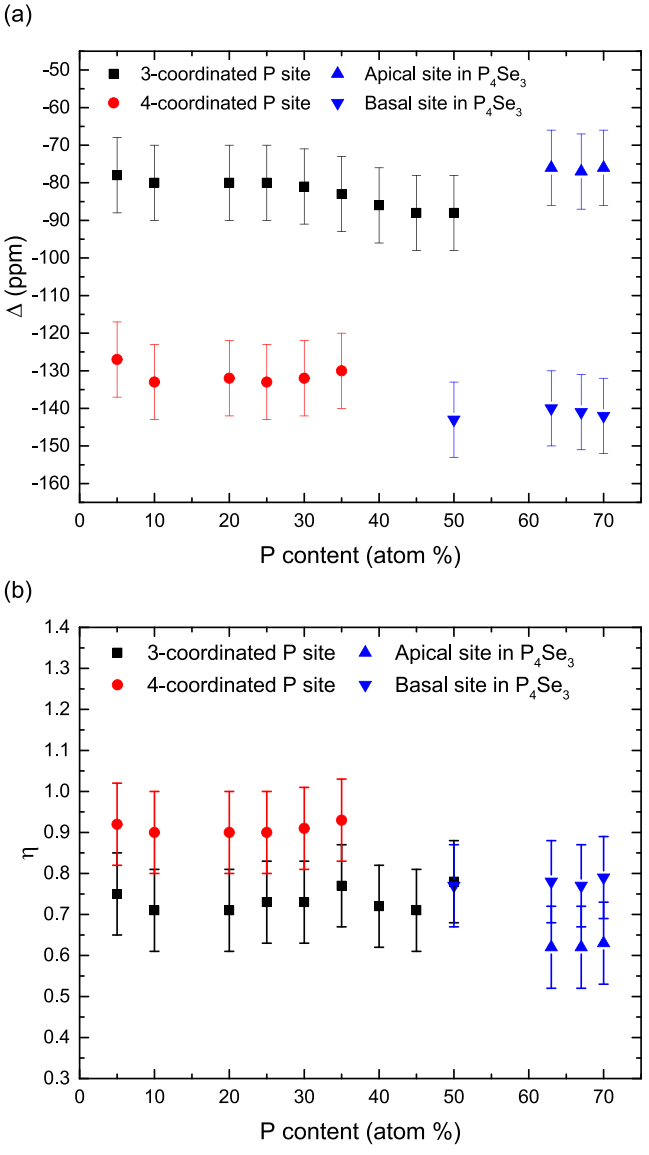

Figure 5. Compositional variation of ^{31}P chemical shift tensor parameters (a) Δ and (b) η for various P sites in P_xSe_{100-x} glasses.

50 can be obtained by integrating the corresponding peak areas. This procedure yields highly accurate speciation results for three- and four-coordinated P environments in these glasses as the isotropic spectra correspond to MAS spectra at infinite spinning speed, which are free from CSA and dipolar coupling related broadening interactions under MAS. The resulting relative fractions of these P environments show smooth variation with composition as the relative fraction of three-coordinated P atoms increases and that of four-coordinated coordinated P atoms decreases with increasing P content (Figure 6). A comparison of these P speciation data with those

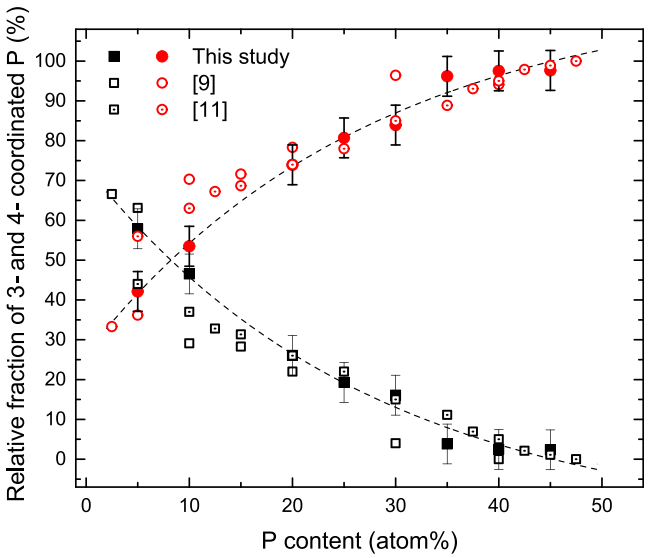

Figure 6. Compositional variation of three-coordinated (filled red circles) and four-coordinated (filled black squares) P site fractions obtained from simulations of ^{31}P isotropic NMR spectra in this study and values reported in the literature from ^{31}P MAS NMR (open symbols).[9,11] Dashed lines through the filled symbols are guides to the eye.

obtained in previous studies using regular 1D ^{31}P MAS NMR (Figure 6) shows reasonable agreement within experimental error except for glasses with $x \leq 20$, where the MAS speciation data show a gentler variation with composition, albeit with a rather large scatter due to the weaker signal:noise of the corresponding spectra.[9,11]

In contrast to P_xSe_{100-x} glasses with $x \leq 50$, the ^{31}P PASS NMR spectra of glasses with $x \geq 63$ are dominated by strong and relatively narrow resonances centered at ∼66 and −74

https://doi.org/10.1021/acs.jpcb.1c07601
J. Phys. Chem. B 2021, 125, 13057−13067

ppm that can be readily assigned, on the basis of their relative area fractions of 1:3, to the apical and basal P sites, respectively, in P_4Se_3 molecules (Figure 3).[25] However, this ratio becomes closer to 1:2 in the ^{31}P PASS NMR spectrum of the $P_{70}Se_{30}$ glass. These two sites differ significantly in their CSA as simulations of the corresponding spinning sideband intensity patterns in the anisotropic dimension yield Δ = 140 (−76) ± 10 ppm and η = 0.8 (0.6) ± 0.1 for the basal (apical) site (Figure 7 and Table 1). It may be noted that these

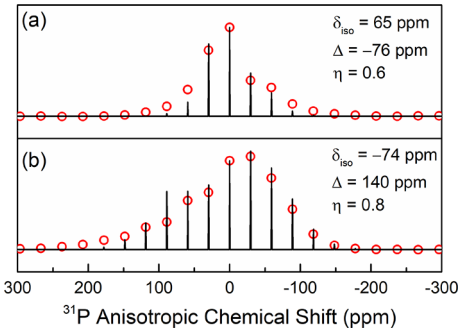

Figure 7. Experimental (empty red circles) and simulated (black traces) ^{31}P NMR spinning sideband intensities in the anisotropic dimension for (a) apical and (b) basal P sites in P_4Se_3 molecules in $P_{63}Se_{37}$ glass, respectively.

resonances, albeit weak, are clearly detectable in the ^{31}P isotropic spectrum of the $P_{50}Se_{50}$ glass, indicating the first appearance of P_4Se_3 molecules in the structure of this glass as P content is increased in the P_xSe_{100-x} system (Figure 3). The ^{31}P NMR spectra of glasses with $x \geq 63$ also contain a broad resonance centered at ∼90 ppm that was assigned in the literature to P atoms in amorphous red phosphorus type environments and three relatively weak resonances near 150, 30, and −125 ppm, which have not yet been conclusively assigned to specific structural units. Based on a recent ^{31}P NMR study of bicyclic P-Se compounds,[26] here, we tentatively assign these resonances near 150, 30, and −125 ppm to the P sites in various isomeric, albeit nonmolecular, P_4Se_3 moieties that are characterized by the opening of the P_3 basal ring in the original P_4Se_3 molecules (Figure 8). This ring opening enables

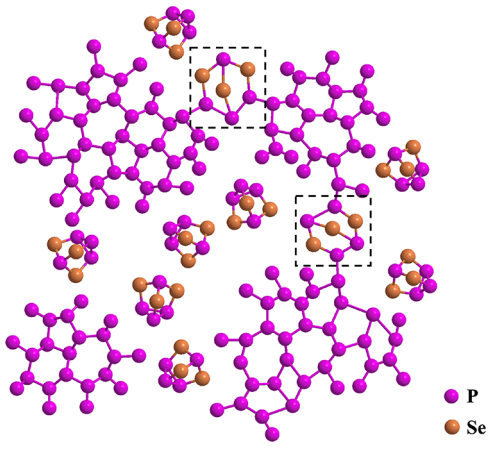

Figure 8. Cartoon showing the structure of P_xSe_{100-x} glasses with $x \geq 63$ consisting primarily of isolated P_4Se_3 molecules and amorphous red phosphorus-like regions with the latter being occasionally cross-linked by P−P bonds with P_4Se_3-like units denoted in dashed boxes.

these moieties to establish connection to the amorphous red phosphorus domains via P−P bonds (Figure 8). This structural scenario is consistent with the observation that the ratio of the apical/basal P sites increases from 1:3 in P_xSe_{100-x} glasses with $x \leq 66.7$ to 1:2 in the $P_{70}Se_{30}$ glass. The formation of such P_4Se_3-like moieties is also consistent with the observation that the Raman spectra of P_xSe_{100-x} glasses with $x \geq 63$ do not show significant change with composition in terms of the appearance of any new band corresponding to the appearance of other distinctly different molecular units (Figure 2). As discussed below, further corroboration of this hypothesis comes from the ^{77}Se MAS NMR spectra of these glasses with $x \geq 63$ (see below). It is interesting to note that, in these high-P glasses, the relative concentrations of the amorphous red phosphorus-like regions and these P_4Se_3-like moieties rise with increasing P content, resulting in an increase in the average structural connectivity as the P content increases from 63 to 70 at % (Figure 3).

3.3. ^{77}Se NMR. The ^{77}Se isotropic NMR spectra of these P_xSe_{100-x} glasses are shown in Figure 9. The spectra of glasses with $x \leq 50$ are dominated by two broad resonances centered at δ_{iso} of ∼853 and ∼700 ppm (Figure 9). However, a self-consistent simulation of these spectral line shapes over this composition range warrants the use of three Gaussian peaks centered at 830−850, 750−760, and 575−630 ppm. These peaks can be assigned to Se−**Se**−Se, Se−**Se**−P and P−**Se**−P environments, respectively.[27] The corresponding simulation parameters are listed in Table 2. It is clear from Table 2 that the intensity of the peak at 830−850 ppm progressively decreases and its δ_{iso} shifts to higher frequencies with increasing P content. A similar shift in ^{77}Se δ_{iso} for this resonance has been observed in the past in the ^{77}Se NMR spectra of Ge−Se and As−Se glasses and can be attributed to the appearance of P as next-nearest neighbors as the Se chain length is shortened due to their progressive cross-linking by P atoms.[28,29] It is interesting to note that the δ_{iso} of the P−**Se**−P resonance shows an even larger shift to higher frequencies with increasing P content compared to that of the Se−**Se**−Se sites (Table 2). It may be recalled that the P speciation in these glasses changes from being predominantly a combination of $Se{=}P(Se_{1/2})_3$ and $P(Se_{1/2})_3$ sites to being dominated by the $_{2/2}SeP{-}PSe_{2/2}$ sites with increasing P content. Consequently, the P−**Se**−P environment becomes increasingly representative of the type that connects the $_{2/2}SeP{-}PSe_{2/2}$ sites forming P−P−**Se**−P−P connections. The high-frequency shift of the P−**Se**−P resonance with increasing P content can therefore be attributed again to the presence of P as next-nearest neighbors. Simulation of the spinning sideband intensity pattern in the anisotropic dimension (Figure 10) yields average CSA tensor parameters of Δ = −151 ± 10 ppm and η = 0.9 ± 0.1 for the Se−**Se**−Se environment and Δ = 290 ± 10 ppm and η = 0.9 ± 0.1 for the P−**Se**−P environment. These ^{77}Se chemical shift tensor parameters for all P_xSe_{100-x} glasses are listed in Table 3 and shown in Figure 11.

In contrast to glasses with $x \leq 50$, the ^{77}Se MAS NMR spectra of P-rich glasses with $x \geq 63$ show only one Se resonance centered at ∼826 ppm (Figure 12). In spite of the similarity in δ_{iso} of this resonance with that of the Se−**Se**−Se environment, the CSA tensor parameters for the former (Δ = −90 ± 10 ppm; η ∼0.3 ± 0.1) are found to be distinctly different from those (Δ = −151 ± 10 ppm; η ∼0.9 ± 0.1) characteristic of the latter (Table 3 and Figures 11 and 13). As shown by the Raman and ^{31}P NMR spectroscopic results,

https://doi.org/10.1021/acs.jpcb.1c07601
J. Phys. Chem. B 2021, 125, 13057−13067

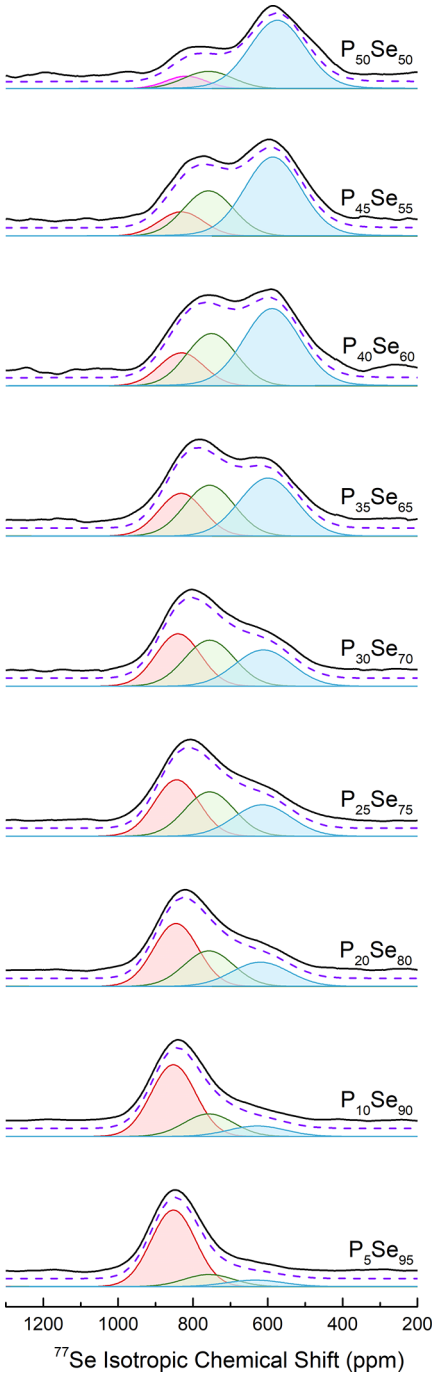

Figure 9. Experimental (solid black line) and simulated (dashed purple line) ^{77}Se isotropic NMR spectra of P_xSe_{100-x} glasses with $x \leq 50$. Individual simulation components for Se−**Se**−Se, Se−**Se**−P, and P−**Se**−P sites are denoted in orange, green, and blue, respectively. The simulation component in pink in the spectrum of $P_{50}Se_{50}$ glass corresponds to P−**Se**−P sites in P_4Se_3 molecules.

P_4Se_3 molecules are major constituents of the structure of these P-rich glasses, and consequently, this Se resonance centered at ∼826 ppm can be assigned to the P−**Se**−P sites in these molecules. This structural assignment is consistent with the previously reported ^{77}Se δ_{iso} (∼800 ppm) for crystalline P_4Se_3 in the literature.[30] Moreover, it is important to note that the width of the ^{77}Se MAS NMR resonance in these high-P glasses progressively increases with increasing P content from 63 to 70 at % (Figure 12). The ^{77}Se MAS NMR spectrum of $P_{63}Se_{37}$ glass displays the narrowest linewidth, which is consistent with a tight distribution of P−Se−P angles and P−Se distances, as would be expected for a molecule such as P_4Se_3. The increased ^{77}Se MAS NMR linewidth in $P_{67}Se_{33}$ and $P_{70}Se_{30}$ glasses indicates an increase in the heterogeneous broadening that can be ascribed to a wider range of P−Se−P angles and P−Se distances that is likely associated with the appearance and increasing concentration of the P_4Se_3-like structural moieties as hypothesized above.

Finally, the compositional variation of the relative fractions of Se−**Se**−Se, P−**Se**−Se, and P−**Se**−P environments in glasses with $x \leq 50$, as obtained from the simulations of the ^{77}Se isotropic NMR spectral line shapes, is shown in Figure 14. The monotonic decrease in the relative fraction of Se−**Se**−Se environments provides evidence in favor of the shortening of Se chains with increasing P content. On the other hand, the P−**Se**−P fraction shows an opposite trend of monotonic increase, while the Se−**Se**−P fraction displays a local maximum at ∼25−30 at % P (Table 2). In order to better understand the spatial distribution and connectivity between the Se−Se and P−Se linkages in the structure, the compositional trend of the Se−**Se**−Se environments is compared with the predictions of several models (Figure 15). Among these models, the chain crossing model assumes that all P-containing structural moieties are separated by at least one Se−Se unit such that no P−Se−P linkages exist, whereas the clustering model assumes that these moieties are all linked together via P−Se−P bridges to form P-rich regions. Clearly, the presence of a significant fraction of Se−**Se**−P sites in these glasses indicates that the clustering model does not accurately describe the connectivity between the Se−Se and P−Se units in these glasses. The random model on the other hand simply considers a random spatial distribution of Se−Se and P−Se units in the glass structure.[17] All model calculations also take into account the presence of the terminal P═Se bond on the $Se{=}P(Se_{1/2})_3$ units and the P−P bond on the $_{2/2}SeP{-}PSe_{2/2}$ units.[17] It is clear from Figure 15 that both random and chain crossing models describe the experimental data well for the Se−**Se**−Se site fractions at low P contents ($x \sim 20$), whereas the experimental data at higher P contents fall between the random and clustering model predictions. This result based on high-resolution ^{77}Se NMR spectra is significantly different from the findings of Maxwell et al., especially for compositions with $x \geq 30$, where their data based on high-temperature ^{77}Se NMR and ^{31}P−^{77}Se SEDOR NMR suggested a random connectivity between the Se−Se and P−Se units.[17] These authors claimed that their Se−**Se**−Se speciation results as obtained from high-temperature ^{77}Se NMR were more accurate than those from SEDOR NMR since the imperfections of the 180° pulse on the ^{31}P channel resulted in less than 100% ^{31}P inversion efficiency for the latter experiments and thus in an overestimation of the Se−**Se**−Se site population. However, we argue that the ^{77}Se isotropic NMR spectra obtained in the present study using 2D ^{77}Se MATPASS/CPMG NMR provide superior resolution and accuracy of selenium speciation compared to the high-temperature ^{77}Se NMR spectra reported by Eckert and co-workers in these pioneering early studies.[17] Therefore, the experimentally observed selenium speciation in these P_xSe_{100-x} glasses with $x \leq 50$ indicates that the spatial distribution of the constituent structural building blocks is best described as intermediate to that predicted by the random and the clustered scenarios. This result can be contrasted with the Se−**Se**−Se

https://doi.org/10.1021/acs.jpcb.1c07601
J. Phys. Chem. B 2021, 125, 13057−13067

Table 2. ^{77}Se NMR Parameters Used for Simulation of ^{77}Se Isotropic NMR Line Shapes[a]

glass composition	P_5Se_{95}	$P_{10}Se_{90}$	$P_{20}Se_{80}$	$P_{25}Se_{75}$	$P_{30}Se_{70}$	$P_{35}Se_{65}$	$P_{40}Se_{60}$	$P_{45}Se_{55}$	$P_{50}Se_{50}$	
					Se−**Se**−Se					
δ_{iso} (±10 ppm)	853	853	846	844	840	832	831	827		
peak width (±10 ppm)	140	140	140	140	140	140	140	140		
relative fraction (±5%)	78	65	47	39	35	24	17	13		
					Se−**Se**−P					
δ_{iso} (±10 ppm)	755	758	758	756	756	756	751	758	759	
peak width (±10 ppm)	155	155	155	155	157	157	157	157	155	
relative fraction (±5%)	14	23	30	34	34	33	30	28	16	
					P−**Se**−P					
δ_{iso} (±10 ppm)	634	629	620	615	612	600	589	587	575	819*
peak width (±10 ppm)	179	179	179	179	179	179	179	178	176	127*
relative fraction (±5%)	8	12	23	27	31	43	53	59	75	9*

[a]Asterisks denote the P−**Se**−P site in P_4Se_3 molecules.

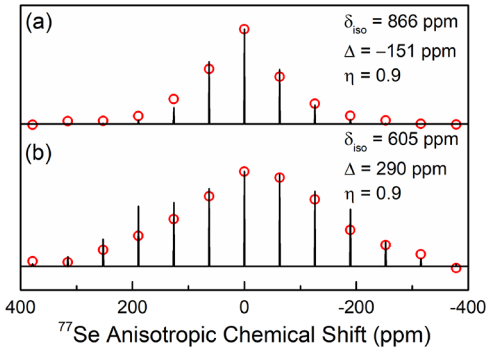

Figure 10. Experimental (open red circles) and simulated (black traces) ^{77}Se NMR spinning sideband intensities in the anisotropic dimension for (a) Se−**Se**−Se sites in P_5Se_{95} glass and (b) P−**Se**−P sites in $P_{30}Se_{70}$ glass, taken at δ_{iso} ~866 and 605 ppm, respectively.

speciation in binary As_xSe_{100-x} glasses, which follows a random distribution as shown in Figure 15.[28] One of the striking features of the P_xSe_{100-x} glasses is the abundance of P−P bonds as exemplified by the ethylene-like $_{2/2}$SeP−PSe$_{2/2}$ units in Se-excess or stoichiometric compositions (P ≤ 40 at %), whereas analogous species are not present in the corresponding As_xSe_{100-x} glasses.[9] In fact, the Raman spectroscopic results presented in this study show that P−P bonds appear for the first time in a highly Se-excess composition with only ~10 at % P. On the other hand, while the structure of the stoichiometric $As_{40}Se_{60}$ glass consists almost exclusively of $AsSe_{3/2}$ pyramids, the structure of the $P_{40}Se_{60}$ glass consists predominantly of $_{2/2}$SeP−PSe$_{2/2}$ units.[9,28]

3.4. Structural Connectivity and Glass Transition Behavior. The T_g of all P_xSe_{100-x} glasses determined in this study are shown in Figure 16. The values are in general in good agreement with those previously reported in the literature.[8,9,31−34] However, it may be noted that, while all glasses prepared in the present study display a single glass transition, Bytchkov et al. reported the observation of two T_g for $P_{67}Se_{33}$ glass.[9] This discrepancy could perhaps be related to a lack of homogenization of the sample during melting in the latter study. The highly nonmonotonic compositional variation of T_g for these glasses as seen in Figure 16 is completely consistent with the corresponding structural evolution. When taken together, the Raman, ^{31}P, and ^{77}Se NMR spectroscopic results indicate that the structural connectivity of the P_xSe_{100-x} glasses increases with progressive addition of P to Se up to $x \sim 50$, at which point the −Se−Se−Se− chain elements disappear and the structure becomes highly rigid. This structural evolution is in accordance with the corresponding increase in T_g with P content in this composition range (Figure 16). The T_g increases slowly up to ~40% P as the Se chains are increasingly cross-linked by P atoms and the average Se chain length decreases. As P content increases to 50 at %, the Se chain elements completely disappear and the structure becomes fully cross-linked via P−Se−P linkages and T_g rapidly increases by ~100 °C (Figure 16). Beyond this point, further addition of P results in the formation of P_4Se_3 molecules, which drastically

Table 3. ^{77}Se Chemical Shift Anisotropy Parameters for P_xSe_{100-x} Glasses

	Se−**Se**−Se site		P−**Se**−P site		P−**Se**−P site in P_4Se_3	
	Δ (±10 ppm)	η (±0.1)	Δ (±10 ppm)	η (±0.1)	Δ (±10 ppm)	η (±0.1)
P_5Se_{95}	−150	0.9	272	0.9		
$P_{10}Se_{90}$	−152	0.9	286	0.9		
$P_{20}Se_{80}$	−154	0.9	288	0.9		
$P_{25}Se_{75}$	−159	0.9	291	0.9		
$P_{30}Se_{70}$	−163	0.9	289	0.9		
$P_{35}Se_{65}$			282	0.9		
$P_{40}Se_{60}$			288	0.9		
$P_{45}Se_{55}$			284	0.9		
$P_{50}Se_{50}$			285	0.9		
$P_{63}Se_{37}$					−82	0.2
$P_{67}Se_{33}$					−92	0.3
$P_{70}Se_{30}$					−100	0.4

https://doi.org/10.1021/acs.jpcb.1c07601
J. Phys. Chem. B 2021, 125, 13057−13067

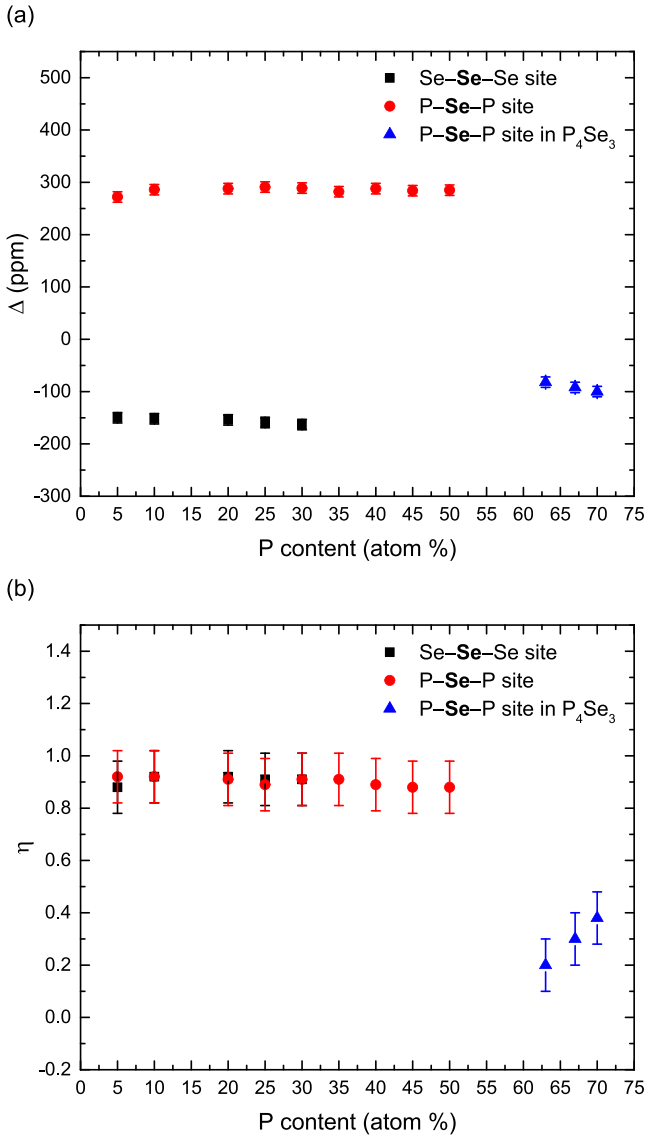

Figure 11. Compositional variation of ^{77}Se chemical shift tensor parameters (a) Δ and (b) η for various Se sites in P_xSe_{100-x} glasses.

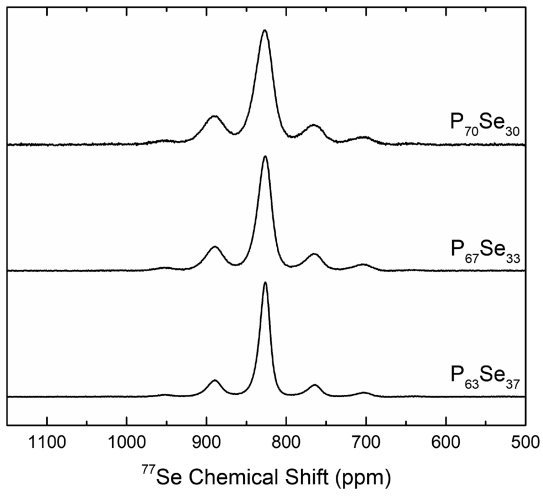

Figure 12. ^{77}Se MAS NMR spectral line shapes of P_xSe_{100-x} glasses with $x \geq 63$. Glass compositions are listed alongside the spectra.

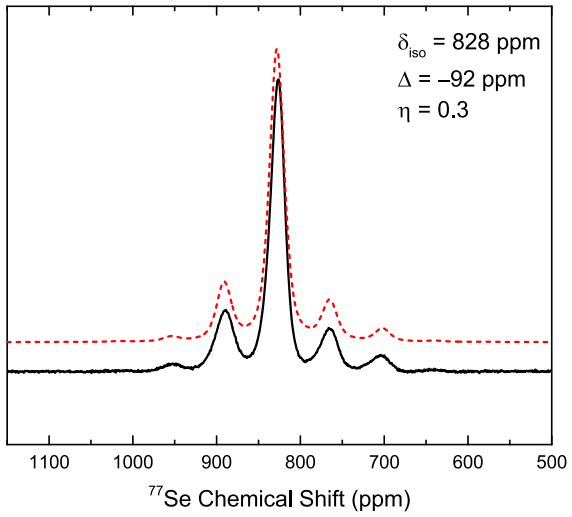

Figure 13. Representative simulation (dotted red line) of ^{77}Se MAS NMR spectrum (solid black line) of $P_{67}Se_{33}$ glass.

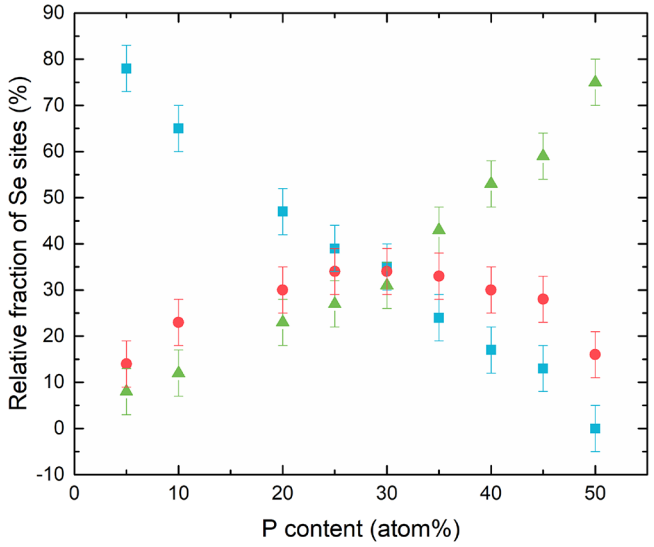

Figure 14. Compositional variation of Se−**Se**−Se (square), Se−**Se**−P (circle), and P−**Se**−P (triangle) site fractions obtained from simulations of ^{77}Se isotropic NMR spectra.

lowers the connectivity of the structure. The concentration of these molecules in these glasses maximizes near $x \sim 63$, and correspondingly T_g decreases by nearly 180 °C. At higher P concentrations, the structural connectivity increases again as the amorphous red phosphorus-like regions become dominant, and consequently, T_g increases by ∼40 °C as P content increases from 63 to 70 at %. This compositional evolution of the structural connectivity and of T_g of P_xSe_{100-x} glasses can be contrasted with that reported in the case of As_xSe_{100-x} glasses by Yang et al.[35] While the P_xSe_{100-x} glasses show a maximum in T_g at $x = 50$, for the As_xSe_{100-x} glasses, this maximum is located at the stoichiometric composition, i.e., at $x = 40$. This difference can be readily attributed to the early appearance of the As_4Se_4 and As_4Se_3 cage molecules in Se-deficient As_xSe_{100-x} glasses with $x > 40$, while the appearance of the P_4Se_3 molecules is delayed in P_xSe_{100-x} glasses until $x > 50$.[35] Moreover, compared to the P_xSe_{100-x} system, near $x \sim 60$, the molecule content appears to remain significantly lower in the

https://doi.org/10.1021/acs.jpcb.1c07601
J. Phys. Chem. B 2021, 125, 13057−13067

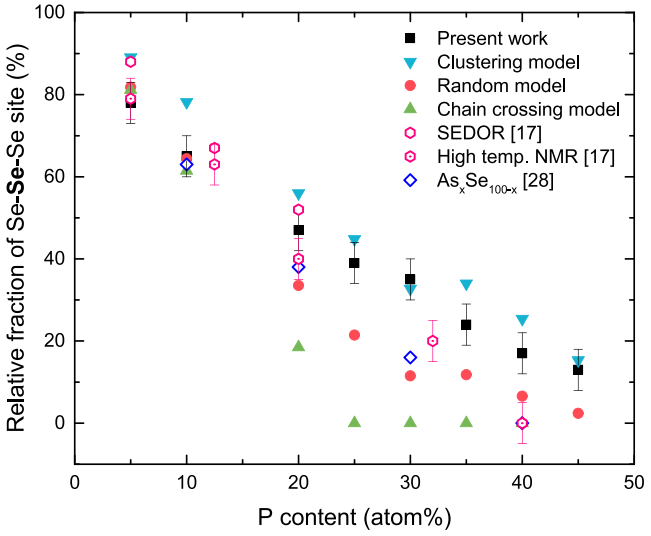

Figure 15. Compositional variation of the Se−**Se**−Se site fraction (squares) compared with that predicted by the clustering (inverted triangles), random (circles), and chain crossing models (triangles). Fractional concentration of the Se−**Se**−Se environment in P−Se (open hexagons) and As−Se (open diamonds) binary glasses reported in previous studies is also included for comparison.[17,28]

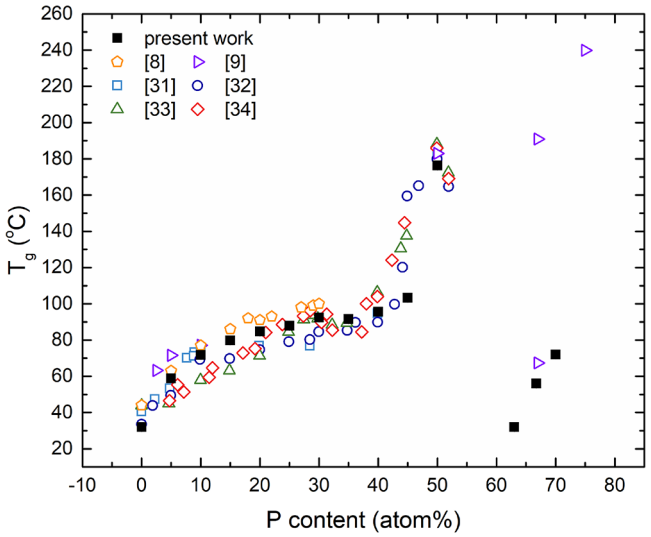

Figure 16. Composition dependence of T_g of binary P_xSe_{100-x} glasses determined in the present study (filled squares) and those reported in the literature (open symbols).[8,9,31−34]

As_xSe_{100-x} glasses, which is consistent with a smaller drop in T_g in the latter.

4. CONCLUSIONS

The compositional evolution of structure and connectivity of P_xSe_{100-x} glasses with $5 \leq x \leq 70$ is studied using a combination of Raman, ^{77}Se, and ^{31}P NMR spectroscopy. Progressive addition of P to Se in glasses with $x \leq 50$ results in cross-linking of Se chains via pyramidal $P(Se_{1/2})_3$ units, ethylene-like $_{2/2}SeP-PSe_{2/2}$ units, and $Se{=}P(Se_{1/2})_3$ tetrahedral units, which ultimately leads to the disappearance of the chain units and the formation of a rigid network structure of corner-shared P-Se polyhedra at $x \approx 50$. Correspondingly, in this composition range, the relative concentration of the Se−**Se**−Se (P−**Se**−P) sites monotonically decreases (increases) with increasing x, and that of the P-Se−Se units goes through a maximum near $x \approx 30$. Additionally, the systematic compositional variation of ^{77}Se δ_{iso} of Se−**Se**−Se and P−**Se**−P sites is found to be related to the number of P atoms as the next-nearest neighbors. The connectivity between the P−Se and Se−Se building blocks in this composition range is best described as intermediate to that of the random and clustered scenarios. The largely connected network of P−Se polyhedra in the $P_{50}Se_{50}$ glass gives way to a structure made primarily of P_4Se_3 molecules held together by van der Waals forces in the $P_{63}Se_{37}$ glass. In fact, the first appearance of these molecules is observed in the ^{31}P NMR spectrum of the $P_{50}Se_{50}$ glass. A further increase in the P content in glasses with $x \geq 63$ results in an increasingly connected network via a decrease in the relative concentration of the P_4Se_3 molecules and the appearance and increase in the concentration of amorphous red phosphorus-like structural moieties and P_4Se_3-like groups that are likely linked via P−P bonds. The overall evolution of the structural connectivity is consistent with the pronounced nonmonotonic compositional variation in T_g.

AUTHOR INFORMATION

Corresponding Author

Sabyasachi Sen − *Department of Materials Science & Engineering, University of California at Davis, Davis, California 95616, United States;* orcid.org/0000-0002-4504-3632; Email: sbsen@ucdavis.edu

Authors

Bing Yuan − *Department of Materials Science & Engineering, University of California at Davis, Davis, California 95616, United States*

Bruce Aitken − *Science & Technology Division, Corning Inc., Corning, New York 14831, United States*

Ivan Hung − *Center of Interdisciplinary Magnetic Resonance, National High Magnetic Field Laboratory, Tallahassee, Florida 32310, United States;* orcid.org/0000-0001-8916-739X

Zhehong Gan − *Center of Interdisciplinary Magnetic Resonance, National High Magnetic Field Laboratory, Tallahassee, Florida 32310, United States;* orcid.org/0000-0002-9855-5113

Complete contact information is available at: https://pubs.acs.org/10.1021/acs.jpcb.1c07601

Notes

The authors declare no competing financial interest.

ACKNOWLEDGMENTS

This work is supported by the National Science Foundation Grant NSF-DMR 1855176. The National High Magnetic Field Laboratory (NHMFL) in Tallahassee, FL, USA, is supported by NSF DMR-1644779 and the State of Florida. Jason Brown is thanked for assistance with glass synthesis.

REFERENCES

(1) Zakery, A.; Elliott, S. R. Optical Properties and Applications of Chalcogenide Glasses: A Review. *J. Non-Cryst. Solids* **2003**, *330*, 1−12.

(2) Bureau, B.; Zhang, X. H.; Smektala, F.; Adam, J. L.; Troles, J.; Ma, H. L.; Boussard-Plèdel, C.; Lucas, J.; Lucas, P.; Le Coq, D.; et al. Recent Advances in Chalcogenide Glasses. *J. Non-Cryst. Solids* **2004**, *345-346*, 276−283.

(3) Calvez, L. Chalcogenide Glasses and Glass-Ceramics: Transparent Materials in the Infrared for Dual Applications. *Comptes Rendus Phys.* **2017**, *18*, 314−322.
(4) Harbold, J. M.; Ilday, F. Ö.; Wise, F. W.; Sanghera, J. S.; Nguyen, V. Q.; Shaw, L. B.; Aggarwal, I. D. Highly Nonlinear As−S−Se Glasses for All-Optical Switching. *Opt. Lett.* **2002**, *27*, 119.
(5) Quémard, C.; Smektala, F.; Couderc, V.; Barthélémy, A.; Lucas, J. Chalcogenide Glasses with High Non Linear Optical Properties for Telecommunications. *J. Phys. Chem. Solids* **2001**, *62*, 1435−1440.
(6) Yu, J.; Zhang, H.; Olsson, E.; Yu, T.; Liu, Z.; Zhang, S.; Huang, X.; Li, W.; Cai, Q. A Novel Amorphous P_4SSe_2 Compound as an Advanced Anode for Sodium-Ion Batteries in Ether-Based Electrolytes. *J. Mater. Chem. A* **2021**, *9*, 12029−12040.
(7) Cao, Y.; Majeed, M. K.; Li, Y.; Ma, G.; Feng, Z.; Ma, X.; Ma, W. P_4Se_3 as a New Anode Material for Sodium-Ion Batteries. *J. Alloys Compd.* **2019**, *775*, 1286−1292.
(8) Georgiev, D. G.; Mitkova, M.; Boolchand, P.; Brunklaus, G.; Eckert, H.; Micoulaut, M. Molecular Structure, Glass Transition Temperature Variation, Agglomeration Theory, and Network Connectivity of Binary P-Se Glasses. *Phys. Rev. B* **2001**, *64*, 134204.
(9) Bytchkov, A.; Fayon, F.; Massiot, D.; Hennet, L.; Price, D. L. ^{31}P Solid-State NMR Studies of the Short-Range Order in Phosphorus-Selenium Glasses. *Phys. Chem. Chem. Phys.* **2010**, *12*, 1535−1542.
(10) Phillips, R. T.; Ellis, M. K. Microstructure of P-Se Glasses and Low Frequency Raman Scattering. *J. Non-Cryst. Solids* **1993**, *164-166*, 135−138.
(11) Lathrop, D.; Eckert, H. Quantitative Determination of the Structural Units in Phosphorus-Selenium Glasses by ^{31} P Dipolar and Magic-Angle-Spinning NMR Spectroscopy. *Phys. Rev. B* **1991**, *43*, 7279−7287.
(12) Lathrop, D.; Eckert, H. Chemical Disorder in Non-Oxide Chalcogenide Glasses. Site Speciation in the System Phosphorus-Selenium by Magic Angle Spinning NMR at Very High Spinning Speeds. *J. Phys. Chem.* **1989**, *93*, 7895−7902.
(13) Lathrop, D.; Eckert, H. Dipolar NMR Spectroscopy of Nonoxidic Glasses. Structural Characterization of the System Phosphorus-Selenium by 31P-77Se Spin Echo Double Resonance NMR. *J. Am. Chem. Soc.* **1990**, *112*, 9017−9019.
(14) Lathrop, D.; Eckert, H. NMR Studies of Chalcogenide Glasses: The System Phosphorus-Selenium. *J. Non-Cryst. Solids* **1988**, *106*, 417−420.
(15) Phillips, R. T.; Wolverson, D.; Burdis, M. S.; Fang, Y. Observation of Discrete Molecular Structures in Glassy P_xSe_{1-x} by Raman Spectroscopy. *Phys. Rev. Lett.* **1989**, *63*, 2574−2577.
(16) Borisova, Z. U. *Glassy Semiconductors*; Springer US , 1981, DOI: 10.1007/978-1-4757-0851-6.
(17) Maxwell, R.; Lathrop, D.; Eckert, H. Intermediate-Range Order in Phosphorus-Selenium Glasses. Constraints from ^{31}P and ^{77}Se NMR Spectroscopy. *J. Non-Cryst. Solids* **1995**, *180*, 244−250.
(18) Hung, I.; Edwards, T.; Sen, S.; Gan, Z. MATPASS/CPMG: A Sensitivity Enhanced Magic-Angle Spinning Sideband Separation Experiment for Disordered Solids. *J. Magn. Reson.* **2012**, *221*, 103−109.
(19) Haeberlen, U. *High Resolution NMR in Solids Selective Averaging: Supplement 1 Advances in Magnetic Resonance*; Elsevier, 2012; Vol. *1*.
(20) Hung, I.; Gan, Z. On the Practical Aspects of Recording Wideline QCPMG NMR Spectra. *J. Magn. Reson.* **2010**, *204*, 256−265.
(21) States, D. J.; Haberkorn, R. A.; Ruben, D. J. A Two-Dimensional Nuclear Overhauser Experiment with Pure Absorption Phase in Four Quadrants. *J. Magn. Reson.* **1982**, *48*, 286−292.
(22) Antzutkin, O. N.; Shekar, S. C.; Levitt, M. H. Two-Dimensional Sideband Separation in Magic-Angle-Spinning NMR. *J. Magn. Reson. Ser. A* **1995**, *115*, 7−19.
(23) Harris, R. K.; Becker, E. D.; Cabral De Menezes, S. M.; Goodfellow, R.; Granger, P. NMR Nomenclature: Nuclear Spin Properties and Conventions for Chemical Shifts (IUPAC Recommendations 2001). *Pure Appl. Chem.* , *2001* (), 1795−1818.
(24) Massiot, D.; Fayon, F.; Capron, M.; King, I.; Le Calvé, S.; Alonso, B.; Durand, J. O.; Bujoli, B.; Gan, Z.; Hoatson, G. Modelling One- and Two-Dimensional Solid-State NMR Spectra. *Magn. Reson. Chem.* **2002**, *40*, 70−76.
(25) Kaseman, D. C.; Gulbiten, O.; Aitken, B. G.; Sen, S. Isotropic Rotation vs. Shear Relaxation in Supercooled Liquids with Globular Cage Molecules. *J. Chem. Phys.* **2016**, *144*, 174501.
(26) Tattershall, B. W.; Sandham, E. L. Interdependence of Phosphorus-31-Selenium-77 NMR Coupling Constants in Bicyclic Phosphorus Selenide Compounds. *J. Chem. Soc. Dalt. Trans.* **2001**, *12*, 1834−1840.
(27) Maxwell, R.; Eckert, H. Molten-State Kinetics in Glass-Forming Systems. A High-Temperature NMR Study of the System Phosphorus-Selenium. *J. Phys. Chem.* **1995**, *99*, 4768−4778.
(28) Kaseman, D. C.; Hung, I.; Gan, Z.; Aitken, B.; Currie, S.; Sen, S. Structural and Topological Control on Physical Properties of Arsenic Selenide Glasses. *J. Phys. Chem. B* **2014**, *118*, 2284−2293.
(29) Kaseman, D. C.; Hung, I.; Gan, Z.; Sen, S. Observation of a Continuous Random Network Structure in Ge_xSe_{100-x} Glasses: Results from High-Resolution ^{77}Se MATPASS/ CPMG NMR Spectroscopy. *J. Phys. Chem. B* **2013**, *117*, 949−954.
(30) Pietraß, T.; Seydoux, R.; Roth, R. E.; Eckert, H.; Pines, A. ^{31}P to ^{77}Se Cross Polarization in β-P_4Se_3. *Solid State Nucl. Magn. Reson.* **1997**, *8*, 265−267.
(31) Borisova, Z.; Kasatkin, B.; Kim, E. Glaeser Im Systemen Phosphor-Selen. *Izv. Akad. Nauk SSSR Neorg. Mater.* **1973**, *9*, 822.
(32) Heyder, F.; Linke, D. Zur Glasbildung in Den Systemen Phosphor-Schwefel Und Phosphor-Selen. *Z. Chem.* **1973**, *13*, 480.
(33) Blachnik, R.; Hoppe, A. Glass Transition and Specific Heats in the Systems P-S, P-Se, As-S and As-Se. *J. Non-Cryst. Solids* **1979**, *34*, 191−201.
(34) Monteil, Y.; Vincent, H. A New Phosphorus Selenide P_4Se_4. *Z. Anorg. Allg. Chem.* **1975**, *416*, 181.
(35) Yang, G.; Bureau, B.; Rouxel, T.; Gueguen, Y.; Gulbiten, O.; Roiland, C.; Soignard, E.; Yarger, J. L.; Troles, J.; Sangleboeuf, J. C.; et al. Correlation between Structure and Physical Properties of Chalcogenide Glasses in the As_xSe_{1-x} System. *Phys. Rev. B* **2010**, *82*, 195206.